Journal of Investigative Surgery

ISSN: (Print) (Online) Journal homepage: https://www.tandfonline.com/loi/iivs20

# Targeting the PANoptosome with 3,4-Methylenedioxy-β-Nitrostyrene, Reduces PANoptosis and Protects the Kidney against Renal İschemia-Reperfusion Injury

Erdal Uysal, Mehmet Dokur, Faruk Kucukdurmaz, Serdar Altınay, Sait Polat, Kadir Batcıoglu, Efe Sezgın, Tuğçe Sapmaz Erçakallı, Aslı Yaylalı, Yakup Yılmaztekin, Zafer Cetın, İlker Saygılı, Osman Barut, Hatem Kazımoglu, Gokturk Maralcan, Suna Koc, Turkan Guney, Nadire Eser, Mehmet Sökücü & Sema Nur Dokur

**To cite this article:** Erdal Uysal, Mehmet Dokur, Faruk Kucukdurmaz, Serdar Altınay, Sait Polat, Kadir Batcıoglu, Efe Sezgın, Tuğçe Sapmaz Erçakallı, Aslı Yaylalı, Yakup Yılmaztekin, Zafer Cetın, İlker Saygılı, Osman Barut, Hatem Kazımoglu, Gokturk Maralcan, Suna Koc, Turkan Guney, Nadire Eser, Mehmet Sökücü & Sema Nur Dokur (2022): Targeting the PANoptosome with 3,4-Methylenedioxy-β-Nitrostyrene, Reduces PANoptosis and Protects the Kidney against Renal İschemia-Reperfusion Injury, Journal of Investigative Surgery, DOI: 10.1080/08941939.2022.2128117

**To link to this article:** https://doi.org/10.1080/08941939.2022.2128117

JOURNAL OF INVESTIGATIVE SURGERY
https://doi.org/10.1080/08941939.2022.2128117

Taylor & Francis
Taylor & Francis Group

ORIGINAL RESEARCH



# Targeting the PANoptosome with 3,4-Methylenedioxy-β-Nitrostyrene, Reduces PANoptosis and Protects the Kidney against Renal İschemia-Reperfusion Injury

Erdal Uysal[a], Mehmet Dokur[b], Faruk Kucukdurmaz[c], Serdar Altınay[d], Sait Polat[e], Kadir Batcıoglu[f], Efe Sezgın[g], Tuğçe Sapmaz Erçakallı[e], Aslı Yaylalı[h], Yakup Yılmaztekin[i], Zafer Cetın[j], İlker Saygılı[k], Osman Barut[l], Hatem Kazımoglu[c], Gokturk Maralcan[a], Suna Koc[m], Turkan Guney[n], Nadire Eser[o], Mehmet Sökücü[p] and Sema Nur Dokur[q]

[a]Department of General Surgery, Sanko University School of Medicine, Gaziantep, Turkey; [b]Department of Emergency Medicine, Biruni University Faculty of Medicine, İstanbul, Turkey; [c]Department of Urology, Sanko University School of Medicine, Gaziantep, Turkey; [d]Deparment of Pathology, Bakırköy Dr Sadi Konuk Health Aplication and Research Center, University of Health Sciences, School of Medicine, İstanbul, Turkey; [e]Department of Histology and Embryology, Çukurova University, Faculty of Medicine, Adana, Turkey; [f]Department of Biochemistry Malatya, Inonu University Faculty of Pharmacy, Battalgazi, Turkey; [g]Izmir Yuksek Teknoloji Enstitusu, Laboratory of Nutrigenomics and Epidemiology, Food Engineering, Izmir Institute of Technology, İzmir, Turkey; [h]Faculty of Medicine, Department of Histology and Embryology and IVF Center, Kahramanmaraş Sütçü İmam University, Kahramanmaraş, Turkey; [i]Faculty of Pharmacy Department of Biochemistry, Inonu University, Malatya, Turkey; [j]Department of Medical Biology, Sanko University School of Medicine, Gaziantep, Turkey; [k]Department of Biochemistry, Sanko University School of Medicine, Gaziantep, Turkey; [l]Department of Urology, Kahramanmaras Sutcu Imam University Faculty of Medicine, Kahramanmaras, Turkey; [m]Department of Anesthesiology and Reanimation, Biruni University Faculty of Medicine, Istanbul, Turkey; [n]Department of Medical Biochemistry, Beykent University, Faculty of Medicine, Istanbul, Turkey; [o]Department of Pharmacology, Kahramanmaraş Sütçü İmam University, Faculty of Medicine, Kahramanmaraş, Turkey; [p]Department of Patology, Sanko University School of Medicine, Gaziantep, Turkey; [q]Faculty of Medicine, Biruni University, Istanbul, Turkey

**ABSTRACT**

**Objectıves:** The objectives of this study were a) to investigate the effect of targeting the PANoptosome with 3,4-methylenedioxy-β-nitrostyrene (MNS) on PANoptosis in the Renal ischemia-reperfussion (RIR) model b) to investigate the kidney protective effect of MNS toward RIR injury.

**Methods:** Thirty-two rats were divided into four groups randomly. The groups were assigned as Control, Sham, DMSO (dimethyl sulfoxide) and MNS groups. The rats in the MNS group were intraperitoneally given 20 mg/kg of MNS 30 minutes before reperfusion. 2% DMSO solvent that dissolves MNS were given to the rats in DMSO group. Left nephrectomy was performed on the rats under anesthesia at the 6th hour after reperfusion. Glutathione peroxidase (GPx), malondialdehyde (MDA), catalase (CAT), superoxide dismutase (SOD) and 8-Okso-2′-deoksiguanozin (8-OHdG) levels were measured. Immunohistochemical analysis, electron microscopic and histological examinations were carried out in the tissues.

**Results:** Total tubular injury score was lower in the MNS group ($p < 0.001$). Caspase-3, Gasdermin D and MLK (Mixed Lineage Kinase Domain Like Pseudokinase) expressions were considerably decreased in the MNS group ($p < 0.001$). Apoptotic index (AI) was found to be low in the MNS group ($p < 0.001$). CAT and SOD levels were higher in the MNS Group ($p = 0.006$, $p = 0.0004$, respectively). GPx, MDA, and 8-OH-dG levels were similar ($p > 0.05$) in all groups. MNS considerably improved the tissue structure, based on the electron microscopic analysis.

**Conclusıons:** Our results suggested that MNS administrated before the reperfusion reduces pyroptosis, apoptosis and necroptosis. These findings suggest that MNS significantly protects the kidney against RIR injury by reducing PANoptosis as a result of specific inhibition of Nod-like receptor pyrin domain-containing 3 (NLRP 3), one of the PANoptosome proteins.

**ARTICLE HISTORY**
Received 16 June 2022
Accepted 17 September 2022

**KEYWORDS**
PANoptosis; PANoptosome; 3,4-methylenedioxy-β-nitrostyrene; ischemia; renal

## Introduction

RIR injury has a complex pathophysiology, including oxidative stress, and acute inflammation. Apoptosis or necroptosis in renal tubular epithelium is the major pathogenesis of acute kidney failure caused by RIR injury. Moreover, pyroptosis, a programmed cell death pathway, also increases renal structural and functional kidney damage [1]. Necroptosis is another pathway of programmed cell death, and it is also associated with RIR damage [2]. Therefore, blocking pyroptosis, apoptosis and necroptosis, and reducing the effects of these pathways, which are an important part

**CONTACT** Erdal Uysal drerdaluysal@hotmail.com Department of General Surgery, Sanko University School of Medicine, Incilipinar Mah. Ali Fuat Cebesoy Bulv. No: 45, 27090 Sehitkamil – Gaziantep, Turkey.

of programmed cell death, could provide a high level of protection against RIR damage.

Recently a novel pathway of proinflammatory programmed cell death, namely PANoptosis has been identified. The name follows the terms of Pyroptosis (P), apoptosis (A) and necroptosis (N) that are regulated simultaneously, and thus called as PANoptosis [3]. PANoptosis is regulated via a recognized cytoplasmic protein complex, the PANoptosome, which initiates three parallel ways of programmed cell death: necroptosis, apoptosis, and pyroptosis [4]. Traditionally, these three pathways were known to affect cell death independently of each other, however, with the discovery of PANOptosis, a link is identified among these three pathways, and the PANoptosome [5, 6].

Because of this interaction, targeting a protein of the PANoptosome that could block the PANoptosis is essential in the formation of RIR damage. In this way, renal damage might be kept to a minimum level by suppressing pyroptosis, apoptosis and necroptosis, simultaneously. Therefore, PANoptosis could be inhibited through interactions in the programmed cell death pathway, especially necroptosis, by selecting MNS as the agent since MNS is a special blocker of NLRP 3, which is one of the PANoptosome proteins.

NLRP3 increases in bacterial infection, and tissue damage. It plays a key role in immune activation and inflammatory response. Reducing NLRP3 activation reduces the inflammation and cellular damage caused by immune response. MSN reduces NLRP3 inflammasome activation by directly binding to NLRP3, and inhibiting ATPase activity. In addition, MNS reduces the IL-1β, IL-18 secretion, caspase-1 levels, and inhibits tyrosine kinases leading to trombosite aggreagtion inhibition. MNS also reduces apoptosis. Due to all these effects, MNS can have protective effect by reducing tissue damage in renal ischemia-reperfussion [7].

Previous studies also suggested the clinical utility of MNS. As NLRP3 activation has a role in inflammatory diseases, MNS is suggested to be a new agent for treatment of inflammatory diseases. Previously, the treatment effects of MNS on cancers such as osteosarcoma has been reported, where MNS induces the apoptosis in tumor cells. MNS plays a role in platelet-dependent thrombosis treatment by inhibiting tyrosine kinase. MNS is therefore suggested to be a potential anti-cancer agent in triple negative breast cancer [7–10].

The present study's objectives were a) to investigate the effect of targeting the PANoptosome with MNS on PANoptosis in the Renal ischemia-reperfussion model and b) to investigate the kidney protective effect of MNS toward RIR injury.

## Materials and methods

Thirty-two female Wistar albino rats were separated at random (10–12 weeks old, and weighed between 200 g and 250 g), into 4 groups, and each group included 8 rats: Control (n: 8), Sham Group (n:8), DMSO Group (Group 3) (n:8), MNS Group (Group 4) (n:8).

### MNS

Commercial MNS is a β-nitrostyrene synthesized from precursor molecules such as piperonal and nitromethane in $C_9H_7NO_4$ isomer formula with a molecular weight of 193.16 gr/mol (United States, National Center for Biotechnology Information, Pubchem). MNS inhibits Syk and Src thyrosine kinases, and NLRP3. MNS is also known as Syk Inhibitor III. It inhibits tubulin polymerization, telomerase activity, and protein phosphotase activity. MNS also inhibits PI3K/AKT/mTOR signaling [8]. MNS is insoluble in water, partially soluble in ethanol, but highly soluble in DMSO and dimethyl formamide. We used DMSO in our study as the solvent. MSN shows its effect within minutes [9]. According to United States Environmental Protection Agency data, the biodegradation half-life of MNS is reported to be 3.55 days. The MNS can be administered intraperitoneally or intravenously. According to U.S. National Library of Medicine data in toxicology studies with mice, MNS toxicity is seen in lower doses when given intravenously, and toxic effects are seen in higher doses when given intraperitoneally. Toxicology studies reported LD50 as 32 mg/kg in intravenous administration. We administered 20 mg/kg MNS intraperitoneally in this study. This dose has been used in the literature, and reported to inhibit NLRP3 [11]. As the administered dose was enough to show inhibitory effects, and risk for toxicity at higher doses only a single dose is administered.

### Surgical technique

The rats were kept in the cages with 18–24 °C temperature and twelve hours of day-night cycle. The selection of female rats in our study was not a special case. However, all rats were synchronized in terms of hormonal cycles. Rats were fed regular rat diet and water. Animal care was conducted in accordance with NIHs publication: "Guide for the care and use of laboratory animals". The rats in Control group were not given any medicines or agents prior to the procedure. The rats in the control group did not undergo renal ischemia and reperfusion. No agent was administered to the rats in the Sham group. Only renal ischemia reperfusion was applied to the rats in this group. The rats in group 3 received 2% DMSO, which dissolves 3,4-methylenedioxy-β-nitrostyrene. DMSO was given intraperitoneally in 2 ml of pysiologic saline 30 minutes before the reperfusion. Rats in group 4 received 20 mg/kg of 3,4-methylenedioxy-β-nitrostyrene (Sigma-Aldrich, St. Louis, MO, USA) dissolved in 2% DMSO. Dissolved 3,4-methylenedioxy-β-nitrostyrene was given intraperitoneally 30 minutes before the reperfusion in 2 ml of pysiologic saline. The 20 mg/kg MNS dose is reported to inhibit NLRP3 inflammasome without toxic effects [11]. Ketamine (Ketalar, Pfizer, USA) 75 mg/kg and 10 mg/kg Xylazine (Rompun, Bayer AG, Leverkusen, Germany) were administered intraperitoneally to the rats as anesthesia. After anesthesia, a 5 cm midline laparotomy was applied to all rats. After opening the abdomen, 10 ml of sterile 0.09% NaCl was administered intraperitoneally for the replacement of lost fluids.

In rats, a short-term ischemia-reperfusion model was developed [12]. According to the ischemia-reperfusion model, left renal peduncle was found and closed with a microvascular clamp. Left renal blood flow was stopped by keeping the renal clamp closed for 45 minutes. The microvascular clamp was then released, allowing renal blood flow to resume. After the kidney color returned to normal, the abdomen of all rats was closed continue with 3/0 silk suture (Doğsan, Istanbul, Turkey). Left nephrectomy was performed on the rats under anesthesia at the 6th hour after reperfusion.

The renal tissues were separated into three pieces, each of which was divided into three equal portions. One of the parts was put in an eppendorf tube and kept at −80 °C until biochemical analysis. For histological evaluation, the other piece was preserved in formaldehyde. The last piece was fixed in glutaraldehyde solution for electron microscopy examination.

## Electron microscopic evaluation

The renal tissue samples were fixed in a five percent glutaraldehyde solution produced with Millonig's phosphate buffer for three hours prior to electron microscopic examination. After shaking two times in the buffer for ten minutes, the samples were fixed in a 1 percent osmium tetraoxide solution prepared with Millonig's phosphate buffer. After 2 hours of osmium tetraoxide fixing, the tissues were washed twice with phosphate buffer for ten minutes each time. After that, the tissues were sequentially dehydrated in 50 percent, 70 percent, 86 percent, 96 percent, and 100 percent of ethyl alcohol (each for 15 minutes). Following that, the tissues were treated with propylene oxide twice for fifteen minutes each time, followed by propylene oxide + resin for thirty minutes each time (twice). The renal tissue pieces were then placed in tubes containing newly prepared embedding material (resin) and swirled for 6 hours in a mixer. The kidney tissue sections were first placed in Beem® tablets the next day using newly manufactured embedding substance, and the material was then polymerized for two days in a 60 °C drying oven. The ultrathin slices (50 nm in thickness) were then cut using a Leica Reichert Ultracut S ultramicrotome (Austria). Saturated uranyl acetate produced in 70% ethyl alcohol and lead citrate solutions were used to stain the sections. Using a Transmission Electron Microscopy (TEM, Japan), the stained slices were examined and micrographed.

## Histopathologic analysis

***Histopathological preparation.*** The rat kidney tissues were sent for pathological examination in 10% buffered formaldehyde solution. The samples were placed in paraffin, and, Hematoxylin and eosin staining was used on 4 µm thinly sliced sections. Preparations were evaluated for histopathological changes under light microscopy (Nikon Ni 50, Japan).

***Histopathological evaluation and grading.*** The histopathological evaluation and grading of the tissue samples were conducted blindly by a board certified pathologist. The extent of kidney damage was determined according to the previously described score system, ranging from 0 to 4 [13].

***Immunohistochemical analysis.*** Immunostaining was done with the Ventana device (Ventana Medical Systems, Inc.). For Caspase-3, Cleaved Caspase-3 (Rabbit Mab#9661, clone no; Asp175, 1/1400 dilution, Cell Marq, USA); for Gasdermin, Cleaved Gasdermin D (Rabbit Mab#36425, clone no; Asp275, E7H9G, 1/1500 dilution, Cell Marq, USA); for MKLK Mouse Mab#3B2, clone no; 293201, 1/1000 dilution, (Santa Cruz Biotechnology Inc, USA) were used. The tissues were deparaffinized in xylene. Manufacturer's instructions were followed for analysis. (Ventana Medical Systems, Inc.).

***Caspase-3 evaluation.*** The standard avidin-biotin peroxidase complex method [14] was followed. Caspase-3 was measured in tissues immunohistochemically. The polyclonal Caspase-3 antibody (Ventana, Roche, USA) was diluted 1:100, and sections were stained by an avibiotin HRP procedure [13].

The following formula was used to determine the Apoptotic Index:

$$\frac{\text{The average amount of cells that are Caspase}-3+\text{ from 5 random areas}}{\text{The average amount of total cells in 5 different areas}}\times 100$$

***Gasdermin D and MLKL evaluation.*** The samples were scored semi-quantitatively to evaluate the immunohistochemical distribution pattern. The staining strength score was graded as follows: 0 (there is no expression), 1+ (light dyeing), 2+ (medium dyeing), 3+ (heavy dyeing). The percentage of cells that were positive for Gasdermin D and MLKL was graded as follows; 0 = negative or uncommon positive cells; 1 = 10 percent of positive cells, 2 = 10–25 percent of positive cells, 3 = 26–50 percent of positive cells, 4 = 51–75 percent of positive cells, 5= >75 percent of positive cells. Immunohistochemical composite score was calculated by multiplying Gasdermin D and MLKL staining strength and staining percentage scores.

## Biochemical studies

We measured the protein concentrations based on the method of Bradford [15]. MDA levels were determined by the Mihara and Uchiyama method [16]. The efficiency of SOD was determined using the Joe M Mccord's previously reported technique [17]. Following the previously established protocol of Luck [18] CAT activity was determined. We determined GPx activity using Lawrence RA's method [19].

The LCMSM technique was used to determine the level of 8-OHdG. It was performed using the DNA isolation method previously described by Gupta [20]. Then the measurement was made spectrophotometrically [21]. After hydrolysis of DNA with formic acid [22] following the protocol described previously [23] instrumental analyzes of 8-OHdG were conducted via a LC–MS/MS system consisting of an Agilent Technologies 1200 series G6460C triple quadrupole (QqQ) HPLC/MS/MS with Jet-StreamW (ESI-MS/MS; Agilent, USA). A Poroshell 120 SB-Aq, 2.7 m, 50 mm, 4.6 mm LC column was injected with six microliters (μL) of the extract. The mobile phase included fifty percent of 5 mM ammonium acetate plus 0.1% acetic acid in water and fifty percent of acetonitrile, respectively. Optimum operating conditions were programmed as follows: sheath gas and auxiliary gas (N2, 99.99%) flow rates are 9 L/min and 8 L/min, respectively; the jacket gas temperature was 400 °C; capillary voltage 3500 V, negative, nozzle voltage 500 V, negative; Six standard solutions of 1, 2, 4, 6, 8, and 10 ppb 8-OHdG in water were evaluated for linearity. Peak areas of 8-OHdG were determined by $R^2 \geq 0.99$. Results were expressed as ng 8-OHdG/mg DNA.

### Statistical analysis

Shapiro-Wilk and Ansari-Bradley tests were used to check the normality and homogeneity of variances assumptions, respectively. Means and their standard deviations (SD) were reported on the tables. One-way ANOVA was used to assess the differences between the groups for variables with normal distribution and non-parametric Kruskal-Wallis test was used for variables with non-normal distribution. Moreover, all pairwise multiple comparisons with the four groups were conducted with Bonferroni correction. For pairwise comparisons, pairwise t-tests and pairwise Wilcoxon tests were conducted for variables with and without normal distribution, respectively. R software (v. 3.6.1) (Organization for Statistical Information, Vienna, Austria) were used for all statistical analyses.

### Ethic statement

The local animal ethics commission (K. University) approved the research (Approval number: 2021/04-03).

## Results

### Electron microscopic evaluation

#### Control group

Electron microscopic evaluation of tissue samples obtained from control group included the fine structures of distal tubule and proximal tubule cells, mesangium, glomerular capillary and visceral epithelial cells (podocytes). The renal tissues in the control group had densely packed mitochondria that mixed with the basal membrane folds and filled the cytoplasm between the basal membranes and nuclei. The renal tissue sections in the control group had a normal morphology, with no evident structural changes in glomerular capillary and mesangial cells (Figure 1a and b).

#### Sham group

Using electron microscopy, tissue samples from the sham group were examined. Following RIR, a detailed analysis of glomerular structure revealed small but significant alterations. Brush boundaries in sham group proximal tubule cells were uncommon and difficult to identify. Membranous whorl structures due to organelle damage was observed in the cytoplasm of tubule cells. Furthermore, in RIR kidneys, the cellular membranes of distal tubule epithelial cells were poorly defined, the basal lamina folds were extremely disordered, and the tightly packed mitochondria were nearly completely displaced. Ubiquitous multivesicular bodies of autophagic vacuoles indicating transition of cells progressing toward death, were observed in tubule cells of the sham group (Figure 2a and b).

#### DMSO group

The fine structure of the tissue samples obtained from the DMSO group showed that in proximal tubule cells although

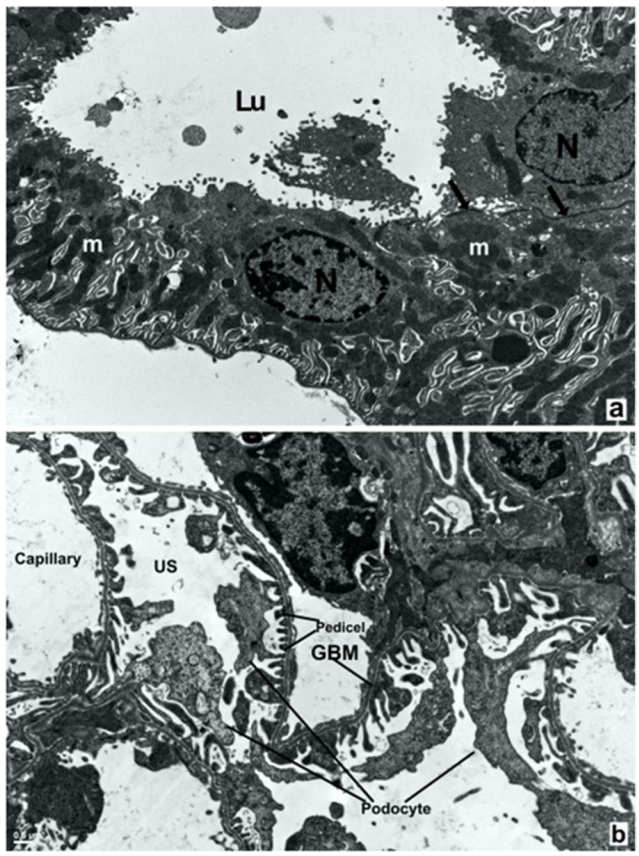


**Figure 1.** Representative transmission electron micrographs of control group; (a) Normal chromatin arrangement in distal tubule cells nuclei (N) are seen. The arrows indicate junctional complex between distal tubule cells. Mitochondria (m) maintain normal fine structure with their cristae and membranes Bar: 1 μm. N, nucleus; Lu, lumen. (b) In glomerulus, podocytes are observed with their foot processes (pedicels) in normal fine structure. Glomerular basement membrane (GBM) lies between podocyte pedicels and capillary endothelial cells Bar: 0,5 μm. US, urinary space.

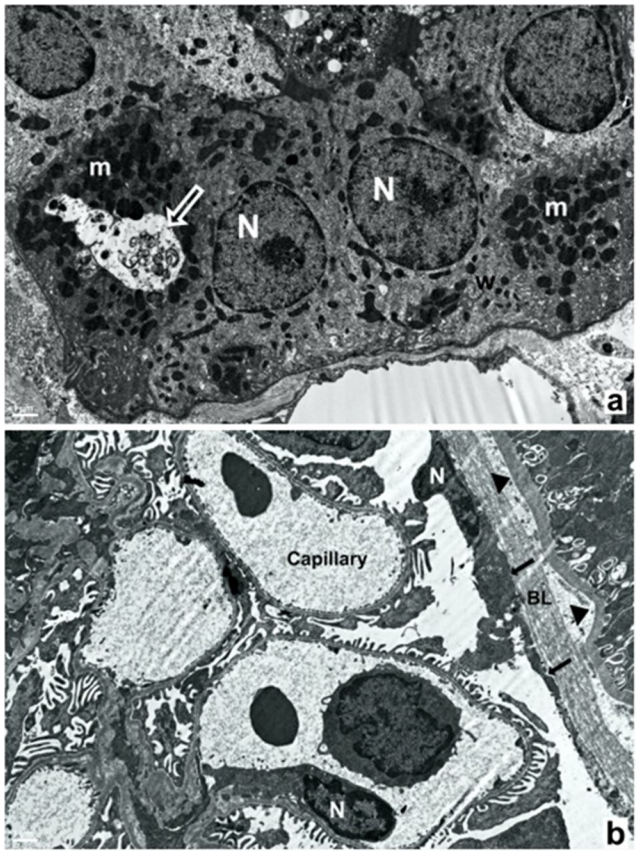


**Figure 2.** Representative transmission electron micrographs of sham group; (c) proximal tubule cells nuclei (N) and mitochondria (m) are seen. The white open arrow indicate autophagic vacuoles symbolizing intracellular digestion as hallmarks of necrosis. Membranous whorl structure (w) due to organelle damage is remarkable. Bar: 1 µm. (d) Diffuse effacement of podocyte pedicels (arrows) and laminated (arrowheads) basement lamina (BL) are noteworthy. Bar: 1 µm. N, nuclei of podocytes.

mitochondria were normal, vacuolization of the cytoplasm was frequently observed. Heterochromatin increase in the nucleus, membranous whorl structures due to organelle damage, residual body in the cytoplasm, increase in edema areas and enlargement in the basal folds were noticed. Furthermore, electron micrographs of the DMSO group revealed normal Bowman's capsule architecture, as well as usual podocytes, mesangial cells, and capsular space in the renal corpuscule (Figure 3a and b).

### MNS treatment group

In the electron micrographs of tissue samples obtained from the MNS group, degenerative changes in the filtration barriers of glomerules and tubular cells were less severe than the sham group. The glomerular basal membrane, mesangial cells and capillary endothelial cells were usually in normal appearance. Degenerative changes in tubular cells were rarely observed. Microvilli of the proximal cells were mostly normal in structure. In distal tubule cells, there were a large amount of mitochondria between the basal folds. Also, lysosomes and lipid droplets were observed in cytoplasm (Figure 4a and b).

### Histopathologic assessment

*Tubular injury*. **Control group:** Minimal cortical changes were seen at a rate of 5% (score 1) in only one of the rats. In other rats, glomeruli and tubules with the usual morphological structure were observed in the cortex and medullary areas. No necrotic and/or degenerative changes were observed. The mean and its standard deviation of the tubular injury score was $0.1 \pm 0.4$ (Table 1).

**MNS group:** Almost no renal damage (score 0) was observed in one of the rats in this group. Minimal score (score 1) was seen in five rats. Histopathological findings reflecting mild (score 2) changes were observed in two of the rats. Scoring range, mean value and standard deviation were 0–2 ($1.1 \pm 0.6$). The score value of the MNS group was significantly lower compared to the Sham group. ($p < 0.001$) (Table 1) (Figure 5).

**Sham group:** Five of the rats in this group had moderate (score 3) renal damage. Histopathological findings reflecting severe (score 4) changes were observed in three of the rats. Scoring range, mean value and standard deviation were founded as 3–4 ($3.4 \pm 0.5$). Sham group's score value was significantly higher compared to the control group ($p < 0.001$) (Table 1) (Figure 5).

**DMSO group:** Mild (score 2) morphology was observed in one of the rats in this group. Based on the histopathological findings, moderate changes were observed in four of the rats (score 3) and severe changes (score 4) in three rats. Scoring range, mean value and standard deviation were recoded as 2–4 ($3.3 \pm 0.70$). There was no statistically significant difference in score values compared to the Sham group. ($p > 0.05$) (Table 1) (Figure 5).

### Immunohistochemical evaluation

*Caspase-3*. The sham and DMSO groups had more significant caspase-3 staining, but the MNS group had less. Caspase-3 staining was negligible in both of the glomeruli, tubuli and interstitial areas in the control group. AI range, mean value and standard deviation was founded as 15–18, $16.3 \pm 1.3$ in the Sham group. AI range, mean value and standard deviation was founded as 2–5, $3.6 \pm 0.9$ in the MNS group. There was a statistically significant difference between the two groups ($p < 0.001$). Similar significance was also obtained for the glomeruli. (Table 1) (Figure 6).

*Gasdermin D*. Only one of the rats in the sham group had moderate (score 2+) staining, while 7 had strong (score 3+) staining. 75% (6/8) of the stainings comprised 50–75% of the kidney parenchyma. Total scoring range, mean value and standard deviation was founded as 6–15, $11.6 \pm 2.50$ in the Sham group. Gasdermin D staining was higher in Sham and DMSO groups, while it was lower in the MNS and Control groups. While there was no staining in 7 rats in the control group, only 1 rat had weak (score 1+) staining. While there was no

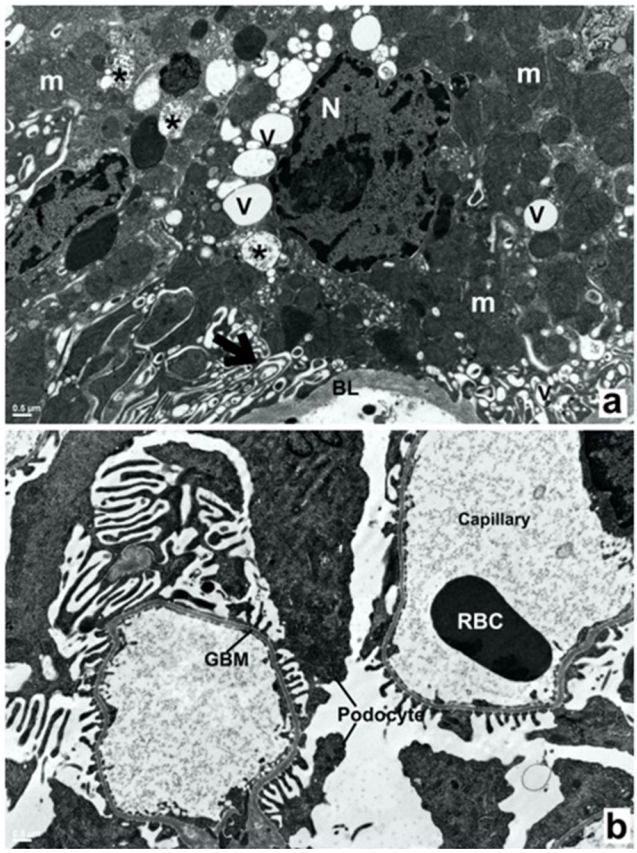


**Figure 3.** Representative transmission electron micrographs of DMSO group; (a) Heterochromatin increase in the nucleus (N) of proximal tubule cells. In cytoplasm of proximal tubule cell, vacuoles (V) and edematous areas (*) are noticed. Arrow indicate enlargement in basal folds. Bar: 0,5 µm. m, Mitochondria; BL, basal lamina. (b) Visceral epithelial cells are seen with their foot processes in normal fine structure Bar: 0,5 µm. GBM, glomerular basement membrane; RBC, red blood cell.

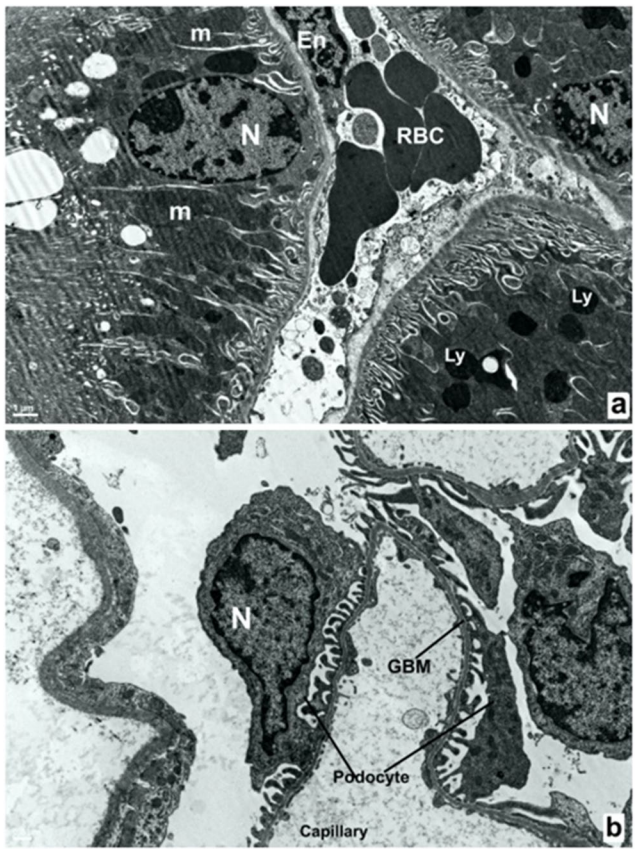


**Figure 4.** Representative transmission electron micrographs of MNS group; (a) It is seen that proximal tubule cells has normal fine structure with nucleus (N) and cytoplasm. Mitochondria (m) and lysosomes (Ly) are noticed in the cytoplasm. Red blood cell (RBC) was seen in peritubuler capillary. Endothelial cell (En) was observed with normal fine structure. Bar: 1 µm. (b) Viseral epithelial cells are seen with their foot processes in normal fine structure Bar: 0,5 µm. GBM, glomerular basement membrane; N, nuclei of podocyte.

**Table 1.** Histopathological and Immunohistochemical comparisons.

| | MNS ($n=8$) | Control ($n=8$) | Sham ($n=8$) | DMSO ($n=8$) | $P$ value[1] |
|---|---|---|---|---|---|
| Apoptotic Index | | | | | |
| *Glomerules* | 1-2 ($1.4\pm0.5$)[a] | 0-1 ($0.3\pm0.5$)[b] | 4-6 ($5.0\pm0.8$)[c] | 3-5 ($4.4\pm0.7$)[c] | < 0.001 |
| *Tubuls* | 2-5 ($3.6\pm0.9$)[a] | 0-1 ($0.3\pm0.5$)[b] | 15-18 ($16.3\pm1.3$)[c] | 15-18 ($16.6\pm1.3$)[c] | < 0.001 |
| Tubular Injury | 0-2 ($1.1\pm0.6$)[a] | 0-1 ($0.1\pm0.4$)[b] | 3-4 ($3.4\pm0.5$)[c] | 2-4 ($3.3\pm0.7$)[c] | < 0.001 |
| Gasdermin D | 0-4 ($1.6\pm1.5$)[a] | 0-0 ($0.0\pm0.0$)[b] | 6-15 ($11.6\pm2.5$)[c] | 8-15 ($11.5\pm2.1$)[c] | < 0.001 |
| MLKL | 1-4 ($2.1\pm1.2$)[a] | 0-0 ($0.0\pm0.0$) [b] | 6-15 ($12.0\pm2.5$)[c] | 8-12 ($9.6\pm1.5$)[d] | < 0.001 |

[1]P values obtained from non-parametric Kruskal-Wallis tests; small letters indicate significantly different groups based on pairwise Wilcoxon tests. Mean ± SD is presented in the parentheses. The small letters a, b, c indicate significantly different groups in statistical comparisons.
MLKL: Mixed Lineage Kinase Domain Like Pseudokinase.
DMSO: Dimethyl sulfoxide, MNS: 3,4-methylenedioxy-β-nitrostyrene.

staining in 1 rat in the MNS group, weak staining was observed in 5 rats (score 1+), and moderate staining was observed in 2 rats (score 2+). 62.5% (5/8) of Gasdermin D Stainings comprised <10% of the kidney parenchyma. Total scoring range, mean value and standard deviation was 0–4, $1.6\pm1.5$ in the MNS group, and the values were significantly lower compared to the sham group ($p<0.001$) (Figure 6) (Table 1).

*MLKL*. Only 3 of the rats in the sham group had medium strength (score 2+) staining, while 5 had strong (score 3+) staining. MLKL staining covered 50–75 percent of the renal parenchyma in 75 percent (6/8) of the rats. Total scoring range, mean value and standard deviation were 6–15, $12\pm2.5$ in the Sham group. MLKL staining was higher in the sham and DMSO groups, while it was lower in the MNS and control groups. While there was no staining in 7 rats in the control group, only one rat had weak (score 1+) staining. In the MNS group, five rats had poor staining (score 1+) and three rats had moderate (score 2+) staining. Total scoring range, mean value and standard deviation were 1–4, $2.1\pm1.2$ in the MNS group,

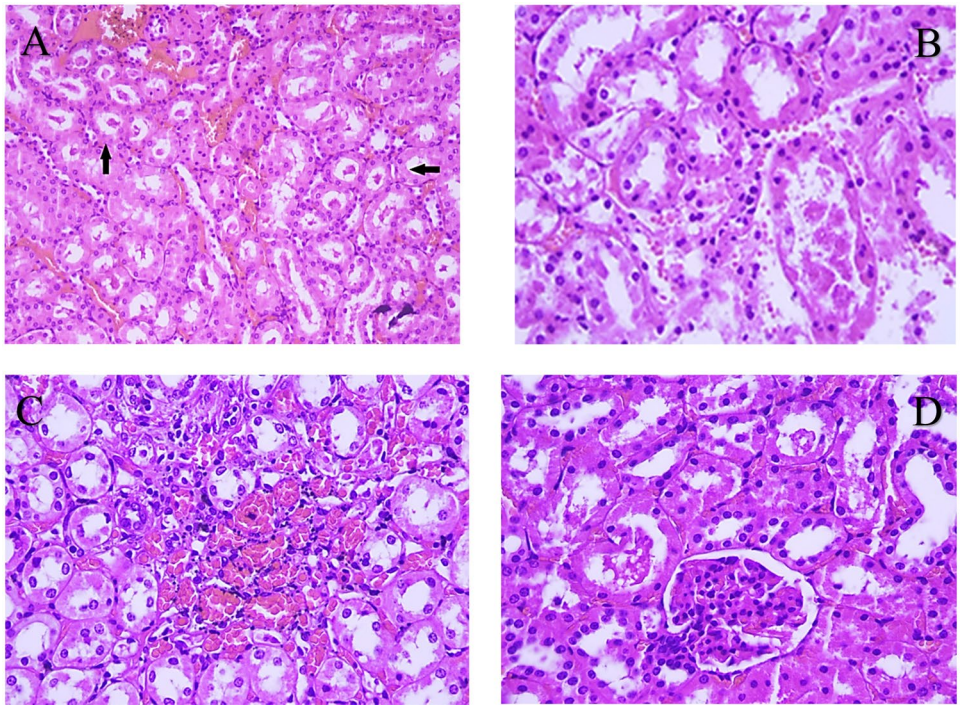


**Figure 5.** Histopathological findings of experimentally induced renal ischemia reperfussion injury. (A) Diffuse eosinophilic casts (black arrows) in tubular lumens and focal interstitial nephritis are seen in sham Group (H&Ex200). (B) Seperation of tubular epithelium, apoptotic bodies indicative of ischemic damage. Sham Group (H&Ex400). (C) Interstitial nephritis finding that did not improve with solution administration in the DMSO Group (H&Ex400). (D) Renal damage appears to be significantly reduced with NLRP3 inhibitor in MNS Group. Please compare with Figure A-B-C and Figure D (H&Ex400).DMSO: dimethyl sulfoxide, MNS: 3,4-methylenedioxy-β-nitrostyrene

and these values were significantly lower compared to the sham group ($p < 0.001$) (Table 1) (Figure 6).

***Biochemical studies***. Significant differences between the groups were observed in terms of the biochemical test results. SOD and CAT values were significantly increased in the MNS and control groups compared to the DMSO and sham groups ($p = 0.006$, $p = 0.0004$, respectively). In terms of GPx MDA and 8-OH-dG levels, no statistical significance was identified between the groups. ($p > 0.05$; Table 2).

## Discussion

In rats in which the RIR model was established, we observed that PANOptosis was reduced by administration of MNS, a strong inhibitor of NLRP 3, one of the PANoptosome proteins. With the decrease of PANoptosis, kidney damage after RIR was found to be significantly lower in rats administrated by MNS in comparison to the those of sham and DMSO groups. Degenerative changes in the filtration barriers of glomerules and tubular cells were less severe than the sham group in the ultrastructural examination performed by electron microscopy. The glomerular basal membrane, mesangial cells and capillary endothelial cells were usually in normal appearance. Degenerative changes in tubular cells were rarely observed. Microvilli of the proximal cells were generally normal in structure. Our results then suggest that MNS significantly protects the kidney from RIR injury in the RIR model. MNS demonstrates this effect via reducing panoptosis through specific inhibition of NLRP 3.

A novel mechanism of proinflammatory planned cell death known as PANoptosis has just been discovered. PANoptosis is controlled by a cytoplasmic protein complex called the PANoptosome. Necroptosis, apoptosis, pyroptosis are managed with PANoptosome control [1]. All three pathways are at the center of the complex events in the pathogenesis of RIR damage [2, 24, 25]. Prior to the introduction of the definition of PANoptosis, it was observed that targeting only one of necroptosis, apoptosis and pyroptosis protected the kidney against RIR damage [24, 26, 27].

After the adoption of PANoptosis concept, necroptosis, apoptosis and pyroptosis are revealed to be interrelated, and they are controlled by the PANoptosome. Therefore, we hypothesized that inhibiting NLRP 3 would reduce PANoptosis and protect the kidney against RIR damage. Thus, MNS, a potent inhibitor of NLRP 3, was chosen for the treatment group (Figure 7).

To the best of our knowledge, the effect of MSN on RIR has not been investigated yet. Moreover, there are no study reported the relationship between PANoptosis and RIR. Thus, the current study is the first study to address all these points. The effects of agents other than MSN on pyroptosis, apoptosis, and necroptosis has been investigated separately. However, the novality of this study is to evaluate pyroptosis, apoptosis, and necroptosis together, and we observed that blocking pyroptosis, apoptosis and necroptosis together reduces the RIR injury.

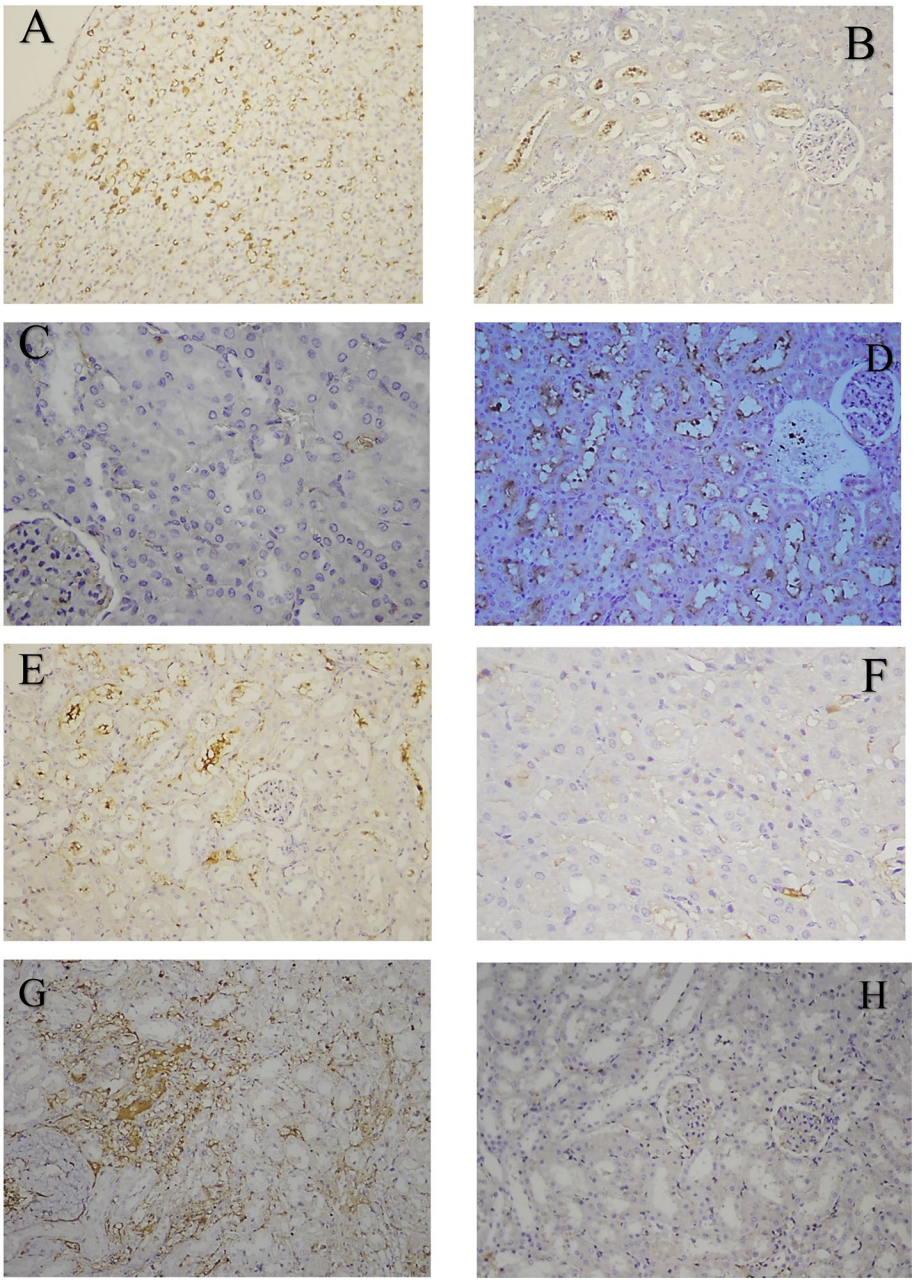


**Figure 6.** Immunohistochemical staining of panapoptotic markers. (A) Caspase-3 staining in Sham group shows high apoptotic index (AI) (x200). (B) Apoptotic cells still appear to be dense in the DMSO Group (x200). (C) Significant reduction of apoptosis due to treatment effect of MNS Group (x400). Only a few cells show Caspase-3 staining. (D) Strong staining of pyroptotic cells in renal injury with Gasdermin D is seen in sham group rats. (x200). (E) Gasdermin D staining of pyroptotic cells is still observed as a weak response in rats in the DMSO group (x200). (F) As an indicator of the MNS treatment effect, only a few cells are stained with Gasdermin D in MNS Group (x400). (G) Significant staining in favor of necroptosis is seen with MLKL in the Sham group (x200). (H) MNS Group shows almost no staining with MLKL, which is the treatment effect of MNS (x200). Please compare with G.DMSO: dimethyl sulfoxide, MNS: 3,4-methylenedioxy-β-nitrostyrene

Apoptosis is an important type of programmed cell death that plays a key role in the pathogenesis of RIR damage. Several complex pathways are activated during apoptosis [28, 29]. Caspase activation is crucial in the initiation of apoptosis. In the apoptosis abortion phase, caspase-3 plays a critical function [30, 31]. Pro-inflammatory cytokines generated through apoptotic pathways are also involved in renal tubule cell death. The release of inflammatory cytokines is also aided by caspase activation. At PANoptosis, caspase-3 is also a marker for apoptosis [30, 32].

In this study, we evaluated apoptosis by calculating the AI through Caspase-3 expiration. When comparing the MNS group to the sham and DMSO groups, the apoptosis index was shown to be considerably lower in both tubular and glomerular cells. Tissue damage is caused by an increase in apoptosis. Li M et al. showed that Caspase-3 was decreased in rats given allicin, and the kidney was protected against RIR damage in this group [31]. Zheng Y et al. reported that Carnosol decreased apoptotic tubular cell death and Caspase 3 activity in their experimental RIR model [33]. In

**Table 2.** Biochemical comparisons.

| Parameter | MNS ($n=8$) | Control ($n=8$) | Sham ($n=8$) | DMSO ($n=8$) | $P$ value[1] |
|---|---|---|---|---|---|
| SOD (U/mg prt) | $6.4\pm3.2^{a}$ | $4.9\pm1.9^{a}$ | $2.8\pm1.0^{b}$ | $3.4\pm1.3^{b}$ | 0.006 |
| GPx (U/mg prt) | $0.19\pm0.08^{a}$ | $0.29\pm0.15^{a}$ | $0.17\pm0.06^{a}$ | $0.12\pm0.05^{a}$ | 0.06 |
| CAT (U/mg prt) | $4573\pm894^{a}$ | $4942\pm2947^{a}$ | $2905\pm573^{b}$ | $3002\pm764^{b}$ | 0.0004 |
| MDA (nmol/mg prt) | $5.8\pm1.6^{a}$ | $4.5\pm0.8^{a}$ | $5.6\pm0.5^{a}$ | $5.8\pm1.4^{a}$ | 0.10 |
| 8-OH-dG (8OHdG ng/mg of DNA) | $1.9\pm1.0^{a}$ | $2.1\pm1.5^{a}$ | $2.4\pm2.3^{a}$ | $3.8\pm2.4^{a}$ | 0.14 |

Mean ± SD are presented.
[1]P values obtained from non-parametric Kruskal-Wallis tests; small letters indicate significantly different groups based on pairwise Wilcoxon tests for non-parametric comparisons. The small letters a and b indicate significantly different groups in statistical comparisons.
SOD: Superoxide dismutase, Gpx: Glutathione peroxidase, CAT: catalase, MDA: Malondialdehyde, 8-OH-dG: 8-Okso-2′-deoksiguanozin, DMSO: dimethyl sulfoxide, MNS: 3,4-methylenedioxy-β-nitrostyrene.

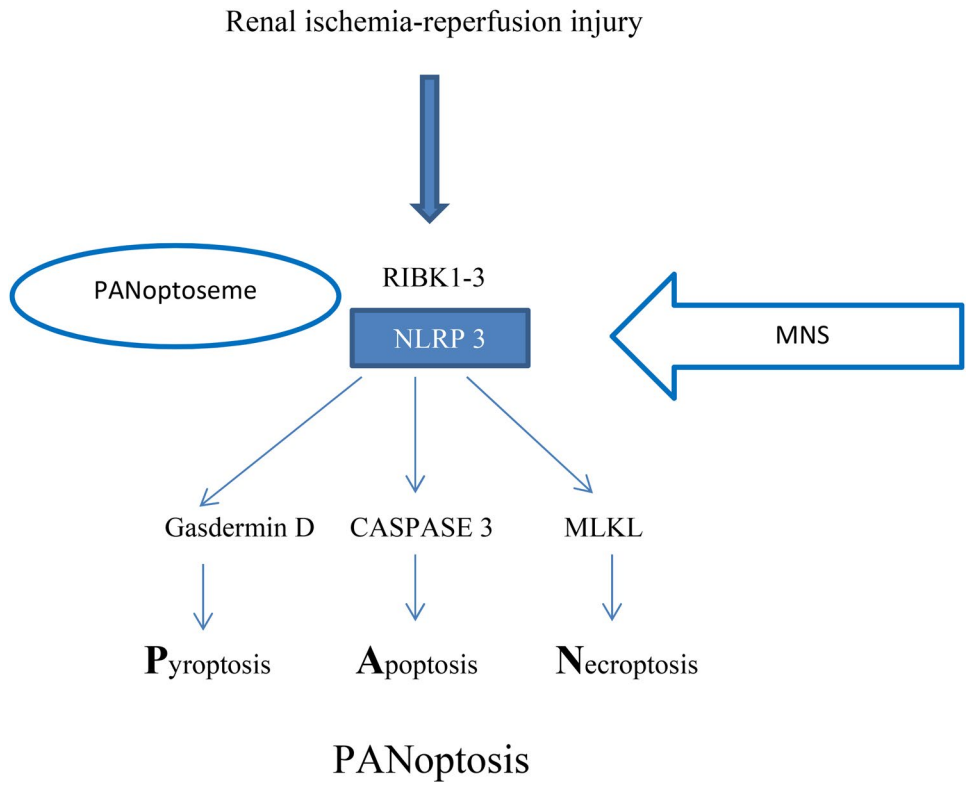


**Figure 7.** Targeting NLRP 3, one of the PANoptoseme proteins, by the MNS.MNS: 3,4-methylenedioxy-β-nitrostyrene, NLRP 3: Nod-like receptor pyrin domain-containing 3, RIBK 1-3: Receptor-interacting protein kinase 1-3, MLKL: Mixed Lineage Kinase Domain Like Pseudokinase

the study of Kang Y et al., RIR damage and apoptosis were reduced with the application of Penehyclidine hydrochloride [34]. Our findings are also consistent with these reports.

Another important mechanism of planned cell death is pyroptosis. Pyroptosis is important in the development of inflammatory tissue damage and has also been linked to RIR [1, 35]. Pyoptosis is triggered by the cytoplasmic protein Gasdermin D, and it is also triggered by the release of interleukin-1. Gasdermin D expression was used to evaluate pyoptosis in our study. When comparing the MNS group to the Sham and DMSO groups, gasdermin D expression was found to be considerably lower in the MNS group. In fact, previous studies showed that decreasing pyroptosis protects cells against cardiac and cerebral ischemia, as well as RIR injury [36, 37]. Tajima T et al. reported that β-hydroxybutyrate protects the kidney against RIR damage through anti-pyroptotic effects [35]. Zhu Y. et al. showed that the kidney was protected against RIR damage by regulating the NLRP3-induced pyroptosis activation of epoxyeicosatrienoic acid in experimental RIR models [38]. The onset of tubular cell destruction is aided by gasdermin D-dependent tubular cell pyroptosis [39]. In the previous experimental RIR model, Wu W. et al., observed that GSDM D-mediated pyroptosis was reduced in the Cholecalciferol group, and the kidney was protected against RIR damage [40]. Furthermore, according to Pang et al., Caspase-1/Gasdermin D-linked pyroptosis reduction in mice given Salvianolic acid B preserved the kidney against RIR injury via activating the Nrf2/NLRP3 signaling pathway [26]. The results obtained in our study are compatible with the findings of these previous studies.

Inflammation is supported by necroptosis, which is a type of programmed cell death. [41]. Moreover, a prior research suggested that necroptosis may be a primary mechanism of cell death in RIR damage, and that inhibiting necroptosis might protect the kidney from RIR damage [2].

Receptor-interacting protein kinase 1–3 (RIPK 1–3) and MLKL are all involved in regulating necroptosis. Furthermore, it is triggered by MLKL phosphorylation by RIPK 3 [41, 42]. MLKL, along with RIPK 1 and RIPK 3, is thought to be a necroptotic marker [2]. RIR damage has also been linked to RIPK-1 acting as a regulator of RIR [24]. Chen et al. found that inhibiting the necroptotic pathway's major components, such as MLKL, RIPK-1, and RIPK-3, lowers RIR damage. Necroptosis mediated by RIPK 3 and MLKL is linked to initial renal damage in RIR injury. Additionally, necroptosis stimulated the activation of the NLRP3 inflammasome [43].

Li C. et al. showed that the kidney was protected against acute kidney injury by blocking necroptosis with a chalcone derivative. Chalcone derivative shows this effect by blocking the RIPK 1, RIPK 3, MLKL signaling pathway [44]. In another experimental study, acute kidney injury caused by RIR or cisplatin administration was reduced in mice given gypenoside XLIX. Gypenoside XLIX was found to exert this effect by means of reducing renal necroptosis [45]. Martens et al. also found that Sorafenib tosylate inhibits RIPK 1 and RIPK 3, and thereby lowers MLKL expression. They demonstrated that this medication, as an inhibitor of TNF-linked necroptosis, prevented the kidney against RIR injury as a result of lowering MLKL expression and necroptosis. [46]. Necroptosis was shown to be lower in the MNS group compared to the sham and DMSO groups in our study. The findings are also consistent with the results of previous studies.

Free oxygen radicals increase in tissue, and cause cell and tissue damage during renal ischemia. Especially, free oxygen radicals' increasing kidney damage through causing lipid peroxidation and tissue damage is more evident during reperfusion [47]. Antioxidant defense mechanisms like GPx, SOD and CAT has a crucial role in protecting against free oxygen radicals [48]. Fatty acid peroxidation causes MDA to be generated in the cell. MDA generation rises in tandem with the rise of free oxygen radicals. MDA generation that is higher than normal suggests oxidative stress. MDA elevation reflects oxidative stress [49]. In previous RIR models, it was observed that the MDA level decreased in the treatment groups, while the activities of antioxidant defense systems such as CAT, SOD, and GPx were increased. Thus, the oxidative stress is reduced and the kidney is protected [50, 51]. In our study, there was no significant difference in MDA levels across the groups. The reason for this may be the fact that MDA cannot rise sufficiently due to the short-term reperfusion period. The high values of MDA occur hours after initiation of reperfusion [49]. In our study, changes may not be observed due to the short-term reperfusion period, and lack of MDA measurements at 12th, 24th and 36 hours after the reperfusion. In addition, various MNS dosages were not used in our research. Aboutaleb et al. obtained different MDA levels with different lavender oil doses in their study on RIR damage [52]. Therefore, future studies examining different MNS doses on MDA levels are still needed to examine the reported dosage effect.

Another indicator of oxidative stress, 8-OH-dG, has been studied as an oxidative stress biomarker. Moreover, 8-OH-dG is the main oxidative lesion originating from free radicals [53]. As shown previously, the level of 8-OH-dG decreases with the reduction of oxidative stress [54, 55]. In the current study, there was no statistical significance between the groups in terms of 8-OH-dG levels. With oxidative stress, 8-OH-dG rises very rapidly in tissue and falls within minutes [56]. These changes could not be observed during our study period. Thus, future studies would alinvestigate the possible effects of different MNS doses and durations on 8-OH-dG.

Antioxidant defense systems such as GPx, CAT, and SOD are thought to protect the kidney against RIR injury. Moreover, during renal ischemia and reperfusion, the levels of CAT, SOD, and GPx drop significantly, while the quantity of free oxygen radicals rises. In fact, boosting CAT, SOD and GPx decreases free oxygen radical damage to cells and tissues. [57, 58]. Previous studies reported the relationships between pyroptosis, apoptosis and lipid peroxidation [59, 60].

The MNS group showed a considerable rise in CAT and SOD levels when compared to the sham and DMSO groups in our study. Although the GPx level was found to be higher in the MNS group compared to the sham and DMSO groups, the result was marginally siginficant ($p = 0.06$). Since our study was designed as the 6-hour short-term reperfusion model, the GPx values obtained after long-term reperfusion such as 24 hours could not be observed. Syng-Ook Lee et al., reported that After performing short-term reperfusion, there was no significant change in GPx levels across the groups [57]. Moreover, in the present study, we did not investigate the efficacy of different MNS dosages. Jiang G. et al. previously investigated the effect of administration of pachymic acid on ferroptosis in mice with RIR. They compared GPx levels between groups after 24 hours of reperfusion. While GPx increase was not significant with low dose pachymic acid, they found a significant increase at high doses [61].

There are some limitations in our study. High MNS doses can reduce ATPase activity, increase NLRP3 inhibition, and significantly reduce inflammatory response [7]. However, in the current study, there was only one dose of MNS administered to rats. As a result, we could not investigate the effectiveness of various dosages. Future research involving the effects of various doses of these medicines on RIR damage would help us understand further on this manner. Moreover, different administration routes may result in different effects. The effects of the intraperitoneal route of administration were observed in our study. In our study, we investigated the results of the short-reperfusion period. Further future research will be needed to determine the efficacy of various ischemia and reperfusion time frames.

## Conclusion

Taking all into consideration, our findings suggest that MNS reduces apoptosis, necroptosis and pyroptosis in the experimental renal ischemia reperfusion model before reperfusion. In addition, tubular damage, glomerular and tubular AI,

gasdermin D, and MLKL expression were all significantly lower in the MNS group. Antioxidant defense system activation, such as SOD and CAT, was found to be increased in the MNS group. In conclusion, inhibition of NLPR 3, one of the PANoptosome proteins, by MNS, reduces PANoptosis and protects the kidney against renal ischemia-reperfusion injury.

## Disclosure statement

No potential conflict of interest was reported by the author(s).

## References


1. Yang JR, Yao FH, Zhang JG, et al. Ischemia-reperfusion induces renal tubule pyroptosis via the CHOP-caspase-11 pathway. *Am J Physiol Renal Physiol*. 2014;306(1):F75–F84. doi:10.1152/ajprenal.00117.2013.
2. Jun W, Benjanuwattra J, Chattipakorn SC, Chattipakorn N. Necroptosis in renal ischemia/reperfusion injury: a major mode of cell death? *Arch Biochem Biophys*. 2020;689:108433. doi:10.1016/j.abb.2020.108433.
3. Malireddi RKS, Kesavardhana S, Kanneganti TD. ZBP1 and TAK1: master regulators of NLRP3 ınflammasome/pyroptosis, apoptosis, and necroptosis (PAN-optosis). *Front Cell Infect Microbiol*. 2019;9:406.
4. Samir P, Malireddi RKS, Kanneganti TD. The PANoptosome: a deadly protein complex driving pyroptosis, apoptosis, and necroptosis (PANoptosis). *Front Cell Infect Microbiol*. 2020;10:238.
5. Christgen S, Zheng M, Kesavardhana S, et al. Identification of the PANoptosome: a molecular platform triggering pyroptosis, apoptosis, and necroptosis (PANoptosis). *Front Cell Infect Microbiol*. 2020;10:237.
6. Meng H, Wu G, Zhao X, et. al. Discovery of a cooperative mode of inhibiting RIPK1 kinase. *Cell Discov*. 2021;7(1):41. doi:10.1038/s41421-021-00278-x.
7. He Y, Varadarajan S, Muñoz-Planillo R, et al. 3,4-methylenedioxy-β-nitrostyrene inhibits NLRP3 inflammasome activation by blocking assembly of the inflammasome. *J Biol Chem*. 2014;289(2):1142–1150. doi:10.1074/jbc.M113.515080.
8. Messerschmitt PJ, Rettew AN, Schroeder NO, et al. Osteosarcoma phenotype ıs ınhibited by 3,4-methylenedioxy-β-nitrostyrene. *Sarcoma*. 2012;2012:479712. doi:10.1155/2012/479712.
9. Wang WY, Wu YC, Wu CC. Prevention of platelet glycoprotein IIb/IIIa activation by 3,4-methylenedioxy-beta-nitrostyrene, a novel tyrosine kinase inhibitor. *Mol Pharmacol*. 2006;70(4):1380–1389. doi:10.1124/mol.106.023986.
10. Chen IH, Chang FR, Wu YC, et al. 3,4-Methylenedioxy-β-n itrostyrene inhibits adhesion and migration of human triple-negative breast cancer cells by suppressing β1 integrin function and surface protein disulfide isomerase. *Biochimie*. 2015;110:81–92. doi:10.1016/j.biochi.2015.01.006.
11. Xiao M, Li L, Li C, et al. 3,4-methylenedioxy-β-nitrostyrene ameliorates experimental burn wound progression by ınhibiting the nlrp3 ınflammasome activation. *Plast Reconstr Surg*. 2016;137(3):566e–575e. doi:10.1097/01.prs.0000479972.06934.83.
12. Chatterjee PK, Patel NS, Kvale EO, et al. The tyrosine kinase inhibitor tyrphostin AG126 reduces renal ischemia/reperfusion injury in the rat. *Kidney Int*. 2003;64(5):1605–1619. doi:10.1046/j.1523-1755.2003.00254.x.
13. Uysal E, Dokur M, Altınay S, et. al. Investigation of the effect of milrinone on renal damage in an experimental non-heart beating donor model. *J Invest Surg*. 2018;31(5):402–411. doi:10.1080/08941939.2017.1343880.
14. Hsu SM, Raine L, Fanger H. The use of antiavidin antibody and avidin-biotin-peroxidase complex in immunoperoxidase technics. *Am J Clin Pathol*. 1981;75(6):816–821. doi:10.1093/ajcp/75.6.816.
15. Bradford MM. A rapid and sensitive method for the quantitation of microgram quantities of protein utilizing the principle of protein-dye binding. *Anal Biochem*. 1976;72:248–254. doi:10.1016/0003-2697(76)90527-3.
16. Mihara M, Uchiyama M. Determination of malonaldehyde precursor in tissues by thiobarbituric acid test. *Anal Biochem*. 1978;86(1):271–278. doi:10.1016/0003-2697(78)90342-1.
17. McCord JM, Fridovich I. Superoxide dysmutase. An enzymic function for erythrocuprein. *J Biol Chem*. 1969;244(22):6049–6055. doi:10.1016/S0021-9258(18)63504-5.
18. Luck H. Catalase. In: Begmeyer HU (ed.) *Methods of enzymatic analysis*. 2nd ed. New York: Academic Press/Verlag Chemie; 1963: 885–94.
19. Lawrence RA, Burk RF. GSH-Px activity in rat liver. *Biochem Biophys Res Commun*. 1976;71(4):952–958. doi:10.1016/0006-291X(76)90747-6.
20. Gupta RC. 32P-postlabelling analysis of bulky aromatic adducts. *IARC Sci Publ*. 1993;(124):11–23.
21. Adachi S, Zeisig M, Möller L. Improvements in the analytical method for 8-hydroxydeoxyguanosine in nuclear DNA. *Carcinogenesis*. 1995;16(2):253–258. doi:10.1093/carcin/16.2.253.
22. Shibayama S, Fujii SI, Inagaki K, et. al. Formic acid hydrolysis/liquid chromatography isotope dilution mass spectrometry: An accurate method for large DNA quantification. *J Chromatogr A*. 2016;1468:109–115. doi:10.1016/j.chroma.2016.09.031.
23. Morgil G, Cok I. Development and validation of a fast and simple LC-ESI MS/MS method for quantitative analysis 8-hydroxyl-2′-deoxyguanosine (8-OHdG) in human urine. *Fabad J. Pharm. Sci*. 2020;45(2):125–134.
24. Shen B, Mei M, Pu Y, et. al. Necrostatin-1 attenuates renal ıschemia and reperfusion ınjury via meditation of HIF-1α/mir-26a/TRPC6/PARP1 signaling. *Mol Ther Nucleic Acids*. 2019;17:701–713. doi:10.1016/j.omtn.2019.06.025.
25. Fawzy MA, Maher SA, El-Rehany MA, et. al. Vincamine modulates the effect of pantoprazole in renal ıschemia/reperfusion ınjury by attenuating MAPK and apoptosis signaling pathways. *Molecules*. 2022;27(4):1383. doi:10.3390/molecules27041383.
26. Pang Y, Zhang PC, Lu RR, et. al. Andrade-oliveira salvianolic acid B modulates Caspase-1-mediated pyroptosis in renal ıschemia-reperfusion ınjury via Nrf2 pathway. *Front Pharmacol*. 2020;11:541426.
27. Karimi Z, SoukhakLari R, Rahimi-Jaberi K, et. al. Nanomicellar curcuminoids attenuates renal ischemia/reperfusion injury in rat through prevention of apoptosis and downregulation of MAPKs pathways. *Mol Biol Rep*. 2021;48(2):1735–1743. doi:10.1007/s11033-021-06214-2.
28. Markó L, Vigolo E, Hinze C, et al. Tubular epithelial NF-κB activity regulates ıschemic AKI. *J Am Soc Nephrol*. 2016;27(9):2658–2669. doi:10.1681/ASN.2015070748.
29. Perry DK, Smyth MJ, Stennicke HR, et. al. Zinc is a potent inhibitor of the apoptotic protease, caspase-3. A novel target for zinc in the inhibition of apoptosis. *J Biol Chem*. 1997;272(30):18530–18533. doi:10.1074/jbc.272.30.18530.
30. Place DE, Lee S, Kanneganti TD. PANoptosis in microbial infection. *Curr Opin Microbiol*. 2021;59:42–49. doi:10.1016/j.mib.2020.07.012.
31. Li M, Ning J, Huang H, Jiang S, Zhuo D. Allicin protects against renal ischemia-reperfusion injury by attenuating oxidative stress and apoptosis. *Int Urol Nephrol*. 2022;54(7):1761–1768. doi:10.1007/s11255-021-03014-2.
32. Meersch M, Schmidt C, Zarbock A. Perioperative acute kidney ınjury: an under-recognized problem. *Anesth Analg*. 2017;125(4):1223–1232. doi:10.1213/ANE.0000000000002369.
33. Zheng Y, Zhang Y, Zheng Y, et al. Carnosol protects against renal ischemia-reperfusion injury in rats. *Exp Anim*. 2018;67(4):545–553. doi:10.1538/expanim.18-0067.
34. Kang Y, Li Y, Wen H, et al. Prevention of renal ischemia and reperfusion injury by penehyclidine hydrochloride through autophagy activation. *Mol Med Rep*. 2020;21(5):2182–2192.
35. Tajima T, Yoshifuji A, Matsui A, et. al. β-hydroxybutyrate attenuates renal ischemia-reperfusion injury through its anti-pyroptotic

effects. *Kidney Int*. 2019;95(5):1120–1137. doi:10.1016/j.kint.2018.11.034.
36. Zhang J, Huang L, Shi X, et. al. Metformin protects against myocardial ischemia-reperfusion injury and cell pyroptosis via AMPK/NLRP3 inflammasome pathway. *Aging (Albany NY)*. 2020;12(23):24270–24287. doi:10.18632/aging.202143.
37. Huang L, Li X, Liu Y, et. al. Curcumin alleviates cerebral ıschemia-reperfusion ınjury by ınhibiting NLRP1-dependent neuronal pyroptosis. *Curr Neurovasc Res*. 2021;18(2):189–196. doi:10.2174/1567202618666210607150140.
38. Zhu Y, Zhu WP, Li W, et al. Implications of EET in renal ischemia/reperfusion by regulating NLRP3 expression and pyroptosis. *Zhonghua Yi Xue Za Zhi*. 2020;100(10):779–784.
39. Miao N, Yin F, Xie H, et al. The cleavage of gasdermin D by caspase-11 promotes tubular epithelial cell pyroptosis and urinary IL-18 excretion in acute kidney injury. *Kidney Int*. 2019;96(5):1105–1120. doi:10.1016/j.kint.2019.04.035.
40. Wu W, Liu D, Zhao Y, et al. Cholecalciferol pretreatment ameliorates ischemia/reperfusion-induced acute kidney injury through inhibiting ROS production, NF-κB pathway and pyroptosis. *Acta Histochem*. 2022;124(4):151875. doi:10.1016/j.acthis.2022.151875.
41. Choi ME, Price DR, Ryter SW, et. al. Necroptosis: a crucial pathogenic mediator of human disease. *JCI Insight*. 2019;4(15):e128834. doi:10.1172/jci.insight.128834.
42. Liu W, Chen B, Wang Y, et. al. RGMb protects against acute kidney injury by inhibiting tubular cell necroptosis via an MLKL-dependent mechanism. *Proc Natl Acad Sci U S A*. 2018;115(7):E1475–E1484.
43. Chen H, Fang Y, Wu J, et. al. RIPK3-MLKL-mediated necroinflammation contributes to AKI progression to CKD. *Cell Death Dis*. 2018;9(9):878. doi:10.1038/s41419-018-0936-8.
44. Li C, Chen QY, He Y, et al. Discovery of a chalcone derivative as potent necroptosis inhibitor for the treatment of acute kidney injury. *Clin Exp Pharmacol Physiol*. 2022;49(8):824–835. doi:10.1111/1440-1681.13670.
45. Yang Q, Zang HM, Xing T, et al. Gypenoside XLIX protects against acute kidney injury by suppressing IGFBP7/IGF1R-mediated programmed cell death and inflammation. *Phytomedicine*. 2021;85:153541. doi:10.1016/j.phymed.2021.153541.
46. Martens S, Jeong M, Tonnus W, et. al. Sorafenib tosylate inhibits directly necrosome complex formation and protects in mouse models of inflammation and tissue injury. *Cell Death Dis*. 2017;8(6):e2904. doi:10.1038/cddis.2017.298.
47. Anaya-Prado R, Toledo-Pereyra LH. The molecular events underlying ischemia/reperfusion injury. *Transplant Proc*. 2002;34(7):2518–2519. doi:10.1016/s0041-1345(02)03471-1.
48. Kataoka T. Study of antioxidative effects and anti-infl ammatory effects in mice due to low-dose X-irradiation or radon inhalation. *J Radiat Res*. 2013;54(4):587–596. doi:10.1093/jrr/rrs141.
49. Bozlu M, Coşkun B, Çayan S, et al. Inhibition of poly (adenosine diphosphata-ribose) polymerase decreases long-term histologic damage intesticular ischemia reperfusion injury. *Urology*. 2004;63(4):791–795. doi:10.1016/j.urology.2003.10.062.
50. Li Y, Hou D, Chen X, et. al. Hydralazine protects against renal ischemia-reperfusion injury in rats. *Eur J Pharmacol*. 2019;843:199–209. doi:10.1016/j.ejphar.2018.11.015.
51. Perez-Meseguer J, Torres-González L, Gutiérrez-González JA, et al. Antiinfl ammatory and nephroprotective activity of Juglans mollis against renal ischemia-reperfusion damage in a Wistar rat model. *BMC Complement Altern Med*. 2019;19(1):186. doi:10.1186/s12906-019-2604-7.
52. Aboutaleb N, Jamali H, Abolhasani M, et al. Lavender oil (Lavandula angustifolia) attenuates renal ischemia/reperfusion injury in rats through suppression of infl ammation, oxidative stress and apoptosis. *Biomed Pharmacother*. 2019;110:9–19. doi:10.1016/j.biopha.2018.11.045.
53. Valavanidis A, Vlachogianni T, Fiotakis C. 8-hydroxy-2'-deoxyguanosine (8-OHdG): a critical biomarker of oxidative stress and carcinogenesis. *J Environ Sci Health C Environ Carcinog Ecotoxicol Rev*. 2009;27(2):120–139. doi:10.1080/10590500902885684.
54. Yan W, Ren D, Feng X, et. al. Neuroprotective and anti-ınflammatory effect of pterostilbene against cerebral ıschemia/reperfusion ınjury via suppression of COX-2. *Front Pharmacol*. 2021;12:770329.
55. Nakayama Y, Ueda S, Yamagishi S, et. al. Asymmetric dimethylarginine accumulates in the kidney during ischemia/reperfusion injury. *Kidney Int*. 2014;85(3):570–578. doi:10.1038/ki.2013.398.
56. Hamilton ML, Guo Z, Fuller CD, et al. A reliable assessment of 8-oxo-2-deoxyguanosine levels in nuclear and mitochondrial DNA using the sodium iodide method to isolate DNA. *Nucleic Acids Res*. 2001;29(10):2117–2126. doi:10.1093/nar/29.10.2117.
57. Lee SO, Chun SY, Lee E, et. al. Renal protective effect of beluga lentil pretreatment for ıschemia-reperfusion ınjury. *Biomed Res Int*. 2021;2021:6890679. doi:10.1155/2021/6890679.
58. Yun Y, Duan WG, Chen P, et. al. Ischemic postconditioning modified renal oxidative stress and lipid peroxidation caused by ischemic reperfusion injury in rats. *Transplant Proc*. 2009;41(9):3597–3602. doi:10.1016/j.transproceed.2009.06.203.
59. Kang R, Zeng L, Zhu S, et al. Lipid peroxidation drives gasdermin D-mediated pyroptosis in lethal polymicrobial sepsis. *Cell Host Microbe*. 2018;24(1):97–108.e4. doi:10.1016/j.chom.2018.05.009.
60. Su LJ, Zhang JH, Gomez H, et al. Reactive oxygen species-ınduced lipid peroxidation in apoptosis, autophagy, and ferroptosis. *Oxid Med Cell Longev*. 2019;2019:5080843.
61. Jiang GP, Liao YJ, Huang LL, et al. Effects and molecular mechanism of pachymic acid on ferroptosis in renal ischemia reperfusion injury. *Mol Med Rep*. 2020;23(1):63. doi:10.3892/mmr.2020.11704.